2010 IEEE International Conference on Robotics and Automation
Anchorage Convention District
May 3-8, 2010, Anchorage, Alaska, USA

Simulation Platform for Self-assembly Structures in MRI-guided Nanorobotic Drug Delivery Systems

Panagiotis Vartholomeos *Member IEEE*, and Constantinos Mavroidis, *Member IEEE*

Abstract— **Magnetic Resonance Imaging (MRI) guided nanorobotic systems that could perform diagnostic, curative and reconstructive treatments in the human body at the cellular and sub-cellular level in a controllable manner have recently been proposed. The concept of a MRI-guided nanorobotic system is based on the use of a MRI scanner to induce the required external driving forces to guide magnetic nanocapsules to a specific target. However, the maximum magnetic gradient specifications of existing clinical MRI systems are not capable of driving superparamagnetic nanocapsules against the blood flow and therefore these MRIs do not allow for navigation. The present paper proposes a way to overcome this critical drawback through the formation of micron size agglomerations where their size can be regulated by external magnetic stimuli. This approach is investigated through modeling of the physics that govern the self-assembly of the nanoparticles. Additionally a computational tool has been developed that incorporates the derived models and performs simulation, visualization and post-processing analysis. Preliminary simulation results demonstrate that external magnetic field causes aggregation of nanoparticles while they flow in the vessel. This is a promising result -in accordance with similar experimental results- and encourages further investigation on the nanoparticle based self-assembly structures for use in nanorobotic drug delivery.**

I. Introduction

Nanorobotic drug delivery systems guided by Magnetic Resonance Imaging (MRI) scanners have been proposed for localized drug delivery in the human body. The expectation is that they will achieve substantially increased rates of therapeutic success compared to conventional methods.

Because of the comparable size with human cells, nanoparticles are the fundamental structure of the nanorobotic concept. Studies have shown that only objects of the size of 30-300 nm can be circulated through the thinnest sections of the vasculature system and would be capable of targeting and interacting with cells [1]. Over the last two decades a variety of nanoparticles and nanovesicle technologies have been developed. Many of these have already been employed for diagnostic and therapeutic purposes [2]. These novel nanoscale platforms are circulated systemically and thus still exhibit poor targeting capabilities. Enhancing the targeting of the nanoparticles necessitates the use of guidance techniques. This in turn, calls for the development of a robotic platform that integrates actuation, sensing and navigation of the nanoparticles.

For this purpose, several groups have employed magnetized micro/ nanoparticles and have implemented magnetic propulsion techniques for the navigation within the vasculature [3, 4]. The favored approach is the use of MRI platform because it is a non-invasive method, it allows for simultaneous actuation and tracking of the nanoparticles, it is capable of providing very accurate localization of the magnetic particles, and commercial MRI devices are readily available at most hospitals. Research on this field has been pioneered since 2003 by Sylvain Martel at the Ecole Polytechnique of Montréal [5, 6]. Another approach is the use of magnetic implants, however its implementation is difficult and medically invasive. Finally, magnetic propulsion techniques other than pulling micro and nanocapsules have also been proposed but these are not MRI compatible [7, 8].

Analysis on the force capabilities of clinical MRI systems demonstrates that they can induce sufficient forces for propelling microparticles but not nanoparticles. This limitation holds even if the MRI platform has been enhanced by special gradient coils. Various solutions have been proposed in the past, including balloon catheter, magnetic implants, larger magnetic carriers, magnetic alloys with stronger magnetization, etc [6]. These approaches suffer from critical drawbacks such as invasive medical procedures, lack of biocompatibility, MRI image distortion.

This paper proposes a novel approach for overcoming the force limitations imposed by the clinical MRI specifications. This approach is the exploitation of the superparamagnetic properties of nanoparticles to stimulate self-assembly processes that yield micron size agglomerations. Furthermore, the paper proposes a modeling framework for the physics that govern the self-assembly formations. Finally, computational tools in MATLAB have been developed that perform simulation, visualization and post

This work was supported by the E.U. FP 7 Program, Research area: ICT -2007.3.6 Micro/Nanosystems under the project NANOMA (Nano-Actuators and Nano-Sensors for Medical Applications), nanoma.zenon.gr.

P. Vartholomeos, is with the company ZENON AUTOMATION TECHNOLOGIES S.A. (www.zenon.gr), and with the Control Systems Lab, Department of Mechanical Engineering, National Technical University of Athens, Greece, (e-mail: barthol@central.ntua.gr).

C. Mavroidis is with the Bionano Robotics Laboratory, Department of Mechanical and Industrial Engineering, Northeastern University, Boston MA02115 USA (phone: 617-373-4121; fax: 617-373-2921; e-mail: mavro@coe.neu.edu)

processing analysis of the nanoparticle in-flow self-assembly process.

II. System Overview

A brief overview of the architecture of a MRI-based robotic nanocapsule drug delivery system is presented in this section. The description highlights (i) the robotic nature of the nanocapsule system; (ii) the physical characteristics of the nanocapsule operating environment and (iii) the MRI-based control system responsible for the navigation of the nanocapsules.

A. The nanocapsule

From a robotics perspective, the nanocapsule is considered as a robotic agent that is part of a "swarm" of agents (i.e. the other nanocapsules). Each agent is composed of components (carbon based structures or molecular elements) that can be categorized into:

- *Actuation elements*. These are the mechanisms responsible for the generation of propulsion forces and torques on the nanocapsule. Actuating elements are usually magnetic nanoparticles that have been encapsulated or attached on the carrier. Typical biocompatible magnetic nanoparticles are made of Fe_3O_4 and usually have dimensions of approximately $10nm$.

- *Sensor elements*. These are mechanisms that sense the status of the environment surrounding the nanocapsule. Such sensing elements – usually based on biomolecules – serve various purposes, like detecting and targeting specific molecules, triggering drug release mechanisms and avoiding immunogenic reactions.

- *Carrier module*. This constitutes the main body (i.e. structural element) of the nanocapsule and serves (i) as the vesicle for loading drug molecules and (ii) as a structure, onto which biomolecules and polymer chains are attached. Existing nanocarrier technologies that could be employed are liposomes, polymer micelles, carbon nanotubes, gold nanoparticles. The size of nanocapsules range from a few tens to a few hundreds nm.

TABLE 1. MAIN TYPES OF ARTERIES [9]

Vessel type	Diameter (m)	Length (m)	U (m/s)
Artery	$3\ 10^{-3}$	$1\ 10^{-1}$	$1\ 10^{-1}$
Small artery	$0.5\ 10^{-3}$	-	$1.3\ 10^{-2}$
Arteriole	$3\ 10^{-5}$	$7\ 10^{-4}$	$1\ 10^{-2}$
Capillary	$7\ 10^{-6}$	$6\ 10^{-4}$	$7\ 10^{-4}$

B. The branching circuit of arteries

The nanoparticles are navigated through the arterial blood distribution system, which branches out into arteries, arterioles and billions of capillaries. At each level of arborization several key parameters vary such as: number of vessels, radius of typical individual vessel, mean linear velocity and pressure profile. For example, the radius of an individual vessel decreases from 1.1 cm in the aorta to a minimum of approximately 3 μm in the smallest capillaries. Blood speed is maximum at the aorta (20-50 cm/s) and minimum at the capillaries (~0.03 cm/s). The blood flow exhibits a pulsate waveform due to the heartbeat. However, this oscillating behavior diminishes as blood moves away from the heart. Table 1 demonstrates typical values for vessel diameter and blood mean speed [9].

C. MRI Based Guidance System Architecture

The architecture of the overall MRI-based drug delivery system is depicted in Fig. 1. The concept of the in-vivo MRI-guidance system is based on the fact that both imaging and propulsion is possible by employing the gradient coils of the MRI system.

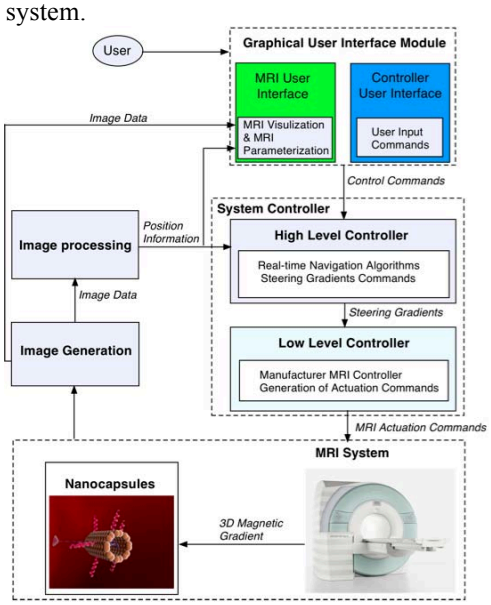

Fig. 1. MRI-based guidance of drug delivery systems.

From a robotics perspective the main components of the guidance system can be categorized as follows:

1) The propulsion module

It is based on the MRI installation and at least contains:

- The Main Magnet. Provides the static magnetic field. For clinical MRIs this is usually 1.5-3T.

- The three Gradient Coils. Generate 3 linearly independent magnetic gradients, which induce controlled actuation forces and torques on the nanoparticles. Clinical MRI systems yield gradients of magnitude that are limited up to 45 mT/m. Insertion of additional special gradient coils (SGC) can increase the gradients up to 450mT/m [6].

2) Tracking Module

In the case of tracking, the gradient coils - described previously - are used for spatial encoding of the MR signals and echo formation. These signals are then processed by a tracking software module that estimates the position and accumulation of the nanocapsules within the vasculature.

3) The Controller Module

Real time control algorithm: High-level controller i.e. endovascular navigation can be accomplished by integrating real-time control algorithms with MRI propulsion system and tracking events. Automatic and stable trajectory tracking require robust controller implementation by "plug-in" control architectures without modifying the hardware of

clinical MRI systems [5,6]. Non-linear controllers for the navigation of micron-sized particles within the blood vessels have already been presented in [10].

III. Propulsion Capabilities of MRI Systems

The purpose of this section is to present the propulsion capabilities and limitations of existing clinical MRI platforms and to identify the optimum hydrodynamic diameter of a particle or agglomeration navigated in the blood vessel. Similar analysis has been performed in the past by [5,6] and focused on an experimental set-up that involves Reynolds number > 1000. In this work, the results are extended for smaller Reynolds numbers $0.01 < \mathrm{Re} < 1000$ often encountered in small arteries, arterioles and capillaries.

For the purpose of the analysis a simplified 1-D model is employed. The dominant forces exerted on a single nanoparticle in a blood vessel are the magnetic force F_m and the blood-flow drag force F_d. These are given by:

$$F_m = VM_s \frac{\partial B_x}{\partial x} \quad (1)$$

$$F_d = 6\pi\eta a U_\infty \quad (2)$$

where V is the volume of the particle (or volume of the agglomeration), M_s is the saturation magnetization of and $\frac{\partial B_x}{\partial x}$ is the magnetic gradient (assuming gradients exist along the x-axis only) and η is the blood viscosity. U_∞ is the relative terminal velocity between fluid and particle velocity in a vessel of infinite diameter and is related to the actual velocity (i.e. the velocity in the vessel of finite diameter) according to the following wall-factor formula [11]:

$$\frac{U}{U_\infty} = \frac{1-\lambda^p}{1+(\frac{\lambda}{\lambda_0})} \quad (3)$$

where U is the actual velocity of the particle and $\lambda = d/l$ is the ratio of particle to vessel diameter. Equation (3) involves two parameters: $p = 1.5$ and $\lambda_0 = 0.29$. The wall-factor formula is important because it incorporates information about the wall effect on the drag force. Gravity and buoyancy forces can be neglected for the case of a single nanoparticle.

The non-dimensional number C_{MD} is defined, here, as the ratio of magnetic forces over drag forces exerted on the particle and is given by:

$$C_{MD} = \frac{F_{mag}}{F_d} = \frac{VM_s}{6\pi\eta r_{cp} U_\infty} \frac{\partial B_x}{\partial x} \quad (4)$$

The critical condition for successful steering is:

$$C_{MD} > 1 \quad (5)$$

The number C_{MD} is plotted against λ for each vessel type of Table 1. A family of curves is produced where each single curve corresponds to a different value of magnetic gradient (up to 50 mT/m for clinical MRIs and above 80 mT/m for preclinical MRIs and SGC insertion). The curves (Fig. 2a-d) have been plotted for U equal to the blood flow. Furthermore, to obtain realistic results it is assumed that the MRI duty cycle is 50% and that the volume fraction of the magnetic material into the nanocapsule is 50%.

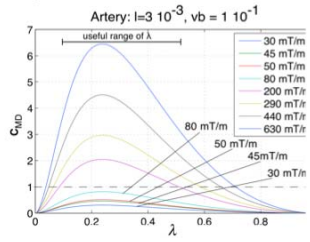

Fig. 2a. C_{MD} vs λ for artery

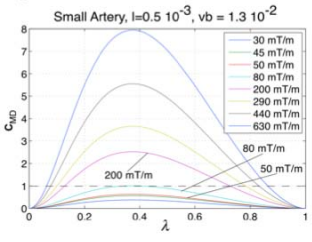

Fig. 2b. C_{MD} vs λ for small artery

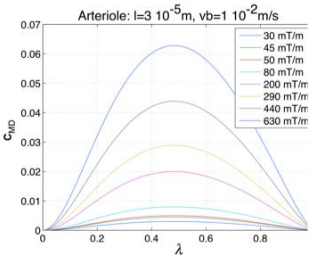

Fig. 2c. C_{MD} vs λ for arterioles

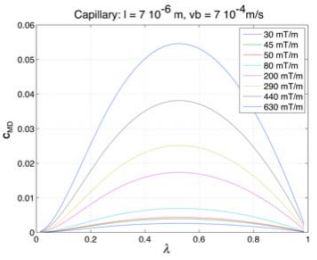

Fig. 2d. C_{MD} vs λ for capillaries

The following observations are made:

(i) Magnetic fields greater than 200 mT/m are required to steer particles of tens of microns against the flow in small and regular arteries.

(ii) No clinical, enhanced clinical or preclinical magnetic gradients can steer nanoparticles against the blood flow in the case of arterioles and capillaries. This is because magnetic forces scale proportional to the particle volume, while drag forces scale proportional to the radius. Hence at the nanoscale magnetic forces are not sufficient to compensate for the drag forces.

(iii) There is an optimum value of λ for each type of vessel. For arteries this is 0.25 and it shifts towards 0.5 at the arterioles and the capillaries. Particles or agglomerations can be steered only if their λ is close to the optimum value. Hence, effective navigation within the artery network requires regulation of the size of the navigated particles (or agglomerations).

Evidently, only clinical MRIs enhanced with special gradient coils can respond to the requirements of magnetic drug delivery and only for microparticles (>50 μm) not for nanoparticles.

An interesting option is to employ biodegradable polymer microvesicles that encapsulate nanoparticles [12]. Although this is a seemingly viable option, it limits the navigation capabilities within the vasculature network due to the fixed volume of the encapsulation polymer microparticle.

In this work a new approach is proposed. This is to investigate the possibility to stimulate self-assembly processes of nanoparticles that yield controlled size

agglomerations. This approach demands detailed modeling of the nanoparticle interaction forces and also demands for efficient computational tools. The following section presents the constructed mathematical models that describe the dominant physical phenomena.

IV. Dynamic Modeling

The model comprises the dominant forces that affect the dynamics of the system of particles. It predicts the motion of each particle as well as the interaction among the particles (magnetic, mechanical, electrostatic). The particles are considered as spheres with viscoelastic properties. The forces taken into account are depicted in the free body diagram of Fig. 3. The bold variables are vectors unless stated otherwise. The Newton-Euler equations are given by:

$$m_i \ddot{\mathbf{v}}_i = \mathbf{F}_{mi} + \mathbf{F}_{cni} + \mathbf{F}_{cti} + \mathbf{F}_{hi} + \mathbf{F}_{bi} + \mathbf{F}_{vdwi} + \mathbf{W}_i \quad (6)$$

$$\mathbf{I}_i \dot{\boldsymbol{\Omega}}_i = \mathbf{M}_{hi} + \mathbf{M}_{ci} + \mathbf{T}_{mi} \quad (7)$$

where the index i indicates particle i. $\dot{\mathbf{v}}_i$ and $\boldsymbol{\Omega}_i$ are the velocity and the angular velocity. The mass is m_i and the mass moment of inertia matrix $\mathbf{I}_i$. $\mathbf{F}_{mi}$ is the total applied magnetic force, $\mathbf{F}_{cni}$ and $\mathbf{F}_{cti}$ are the normal and tangential contact forces respectively, $\mathbf{F}_{bi}$ and $\mathbf{W}_i$ are the buoyancy and the weight forces, $\mathbf{F}_{hi}$ is the hydrodynamic drag force and $\mathbf{F}_{vdwi}$ is the van der Waals force. $\mathbf{M}_{hi}$ and $\mathbf{M}_{ci}$ are the hydrodynamic moments and the contact moments respectively. $\mathbf{T}_{mi}$ is the torque due to the magnetic field at the position of particle i. Particles are considered large enough to neglect the effect of Brownian motion.

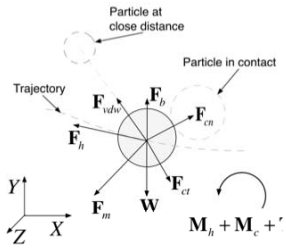

Fig. 3. Free body diagram of a single particle.

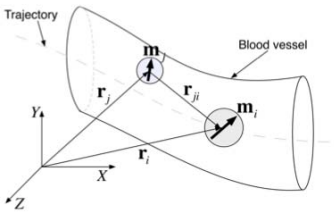

Fig. 4 Configuration of particle-to-particle magnetic interaction.

A. Magnetic forces

Modeling particle-particle magnetic interaction is critical for predicting the self-assembly formations of the magnetized nanoparticles. Due to the small size of the nanoparticles it is assumed that the spatial variation of the field over the particle diameter is small compared to the average field. Hence, each particle is magnetized uniformly and behaves like a dipole placed at the center of the sphere (Fig. 4). In this case the magnetic forces and torques exerted on a particle i, at position $\mathbf{r}_i$, are given by:

$$\mathbf{F}_{mi} = (\mathbf{m}_i \cdot \nabla)\mathbf{B}_i \quad (8)$$

$$\mathbf{T}_{mi} = \mathbf{m}_i \times \mathbf{B}_i \quad (9)$$

where $\mathbf{m}_i$ is the magnetic moment of particle i and ∇ is the gradient operator. $\mathbf{B}_i$ is the total magnetic field at particle i and is given by:

$$\mathbf{B}_i = \mathbf{B}_{0i} + \sum_{\substack{j \\ j \neq i}}^{N} \mathbf{B}_{ji} \quad (10)$$

where $\mathbf{B}_0$ is the external magnetic field applied at particle i and $\mathbf{B}_{ji}$ is the field at the i^{th} particle due to the magnetic moment of particle j placed at position $\mathbf{r}_j$. N is the total number of particles. Then $\mathbf{B}_{ji}$ is given by [13]:

$$\mathbf{B}_{ji} = \frac{\mu_0}{4\pi}\left[\frac{3(\mathbf{m}_j \cdot \mathbf{r}_{ji})}{|\mathbf{r}_{ji}^5|} - \frac{\mathbf{m}_j}{|\mathbf{r}_{ji}^3|}\right] \quad (11)$$

where $\mathbf{r}_{ji}$ is as demonstrated in Fig. 4. The particles exhibit superparamagnetic properties, i.e. they are hysteresis-free and for zero applied magnetic field they exhibit zero net magnetization. In this case the magnetic moment $\mathbf{m}_i$ of particle i is given by:

$$\mathbf{m}_i = \frac{4\pi}{\mu_0}\frac{\mu_r - 1}{\mu_r + 2}\frac{d_i^3}{8}\mathbf{B}_i \quad (12)$$

where μ_r is the relative permeability of the superparamagnetic i^{th} particle, and d_i its diameter. Substituting Eqs. (10) and (11) into Eq. (12) results in a linear system of $2N$ equations and $2N$ unknowns. Solving the system yields the magnetic moment $\mathbf{m}$ of each particle. The $\mathbf{m}$ vectors are substituted back into Eqs. (10) and (11) to yield the magnetic forces applied on each particle.

B. Contact forces

Contact force models, are critical for predicting the formation and the size of the agglomerations and also for predicting their breakup processes due to the shear flow. In the latter case the key concept is to model the propagation of the drag and shear forces through the particles agglomeration. The modeling method used in this paper is the Discrete Element Modeling (DEM). This method exploits the viscoelastic properties of spheres and provides an excellent tool for moderate size problems (up to ~10^4). In these calculations movements due to all of the contact forces from neighboring particles are accounted for. The general modeling method is described in detail in [14]. What follows is a brief presentation of the basic modeling elements used in the nanoparticle system model.

Particles in a DEM problem are physically approximated as rigid bodies and the contacts between them, as contact points. The contact takes place if and only if the following condition holds:

$$(a_i - a_j) - \left\|\mathbf{r}_i - \mathbf{r}_j\right\| > 0 \quad (13)$$

where a_i, a_j are the radii of the spheres i and j.

The collision between particle i and j generates at the contact point a contact force $\mathbf{F}_{ci}$ on particle i (and

respectively a force $\mathbf{F}_{cj} = -\mathbf{F}_{ci}$ on particle j). $\mathbf{F}_{ci}$ is resolved on the normal $\mathbf{n}_{ji}$ and tangential $\mathbf{t}_{ji}$ unit vectors (Fig. 5a) to yield the normal $\mathbf{F}_{cni}$ and tangential $\mathbf{F}_{cti}$ forces. The normal and tangential unit vectors are given by:

$$\mathbf{n}_{ji} = (\mathbf{r}_i - \mathbf{r}_j) / \left|\mathbf{r}_i - \mathbf{r}_j\right| \tag{14}$$

$$\mathbf{t}_{ji} = \mathbf{v}_{ji} / \left|\mathbf{v}_{ji}\right| \tag{15}$$

where $\mathbf{v}_{tji}$ is the tangential relative velocity of sphere i with respect to sphere j:

$$\begin{aligned}\mathbf{v}_{tji} &= \mathbf{v}_i - \mathbf{v}_j - [(\mathbf{v}_i - \mathbf{v}_j)\cdot \mathbf{n}_{ji}]\mathbf{n}_{ji} \\ &-a_i \mathbf{n}_{ji} \times \Omega_i - a_j \mathbf{n}_{ji} \times \Omega_j\end{aligned} \tag{16}$$

where Ω_i, Ω_j are the angular velocities of the spheres i, j.

$\mathbf{F}_{cni}$ and $\mathbf{F}_{cti}$ are represented by a Voigt model comprising a non-linear spring and a linear damper (see Fig. 5b and c). Dry friction of nanoparticles has being neglected.

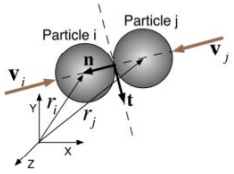

Fig. 5a. Collision.

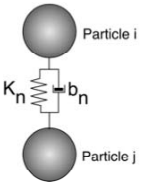

Fig. 5b. Normal forces.

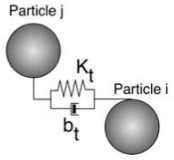

Fig. 5c. Tangential forces.

The normal contact force is given by:

$$\mathbf{F}_{c\_ni} = (k_{ni}\xi_i^{3/2} + b_{ni}\dot{\xi}_i)\mathbf{n}_i \tag{17}$$

where the first term is the elastic force –based on the Hertz contact law for spherical particles- and the second is the viscous force. The variable ξ_i represents the elastic deformation of sphere i at the contact point of spheres i and j.

The tangential contact force on sphere i is given by:

$$F_{\tau i} = (k_{\tau i}\zeta_i + b_{\tau i}\dot{\zeta}_i)\mathbf{t}_{ji} \tag{18}$$

where ζ_i is the displacement in the tangential direction that took place since the instant of contact.

Slight modification of the aforementioned elements allows modeling also the interaction between particles and the vessel walls. In this case the wall is considered rigid body along the tangential direction and deformable along the normal direction. Furthermore, the method can be used to model geometries other than spheres, by approximately composing their geometries by a rigid collection of overlapping spheres.

For DEM simulations the integration time step is chosen to produce 10 and 20 time steps over the timespan of a typical collision, often with very low order integration schemes.

C. Fluid forces

The hydrodynamic force and torque on each particle are based on the Stokes drag force for a sphere and are given by:

$$\mathbf{F}_{hi} = \lambda_{fi} 6\pi\eta(2a)(\mathbf{E}\cdot\mathbf{p}_i - \mathbf{v}_i) \tag{19}$$

$$\mathbf{M}_{hi} = \lambda_{mi} 8\pi\eta(2a)^3(\Omega_0 - \Omega_i) \tag{20}$$

where, η is the viscosity of the blood and depends on several parameters such as vessel diameter, hematocrite, etc. [15]. $\mathbf{P}_i$ is the position vector of the particle resolved on the local frame attached to the longitudinal axis of the vessel as shown in Fig. 6. $\mathbf{E}$ and Ω_0 are the velocity gradient tensor and vorticity vector of the flow field respectively and for a 2-D shear flow case are given by:

$$\mathbf{E} = \begin{bmatrix} 0 & \gamma_s & 0 \\ 0 & 0 & 0 \\ 0 & 0 & 0 \end{bmatrix}, \Omega_0 = \begin{bmatrix} 0 & 0 & -\frac{\gamma_s}{2} \end{bmatrix} \tag{21}$$

where γ_s is the shear rate of laminar flow in the vessel (see Fig. 6) given by:

$$\gamma_s = \overline{v}_f \frac{p_{iy}}{(l/2)^2} \tag{22}$$

$\overline{v}_f$ is the mean the speed flow and l is the vessel diameter.

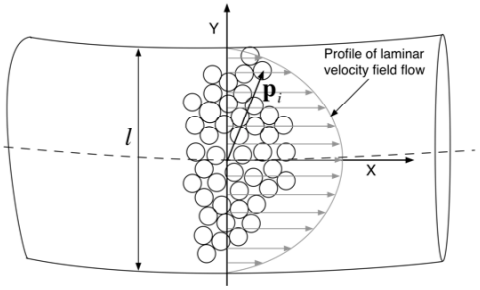

Fig. 6. Particle aggregation into blood vessel.

The parameters $\lambda_{fi}, \lambda_{mi}$ are correction factors that account for the fact that not all spheres are completely exposed to the fluid drag forces. This correction is important for highlighting the disproportional variation of magnetic and drag forces as the scale changes. Algorithms for their determination can be found in the literature [14].

D. Gravitational forces

These include the force due to gravity and the force due to buoyancy. Although of limited effect at the nanoscale, they might become important when micron size aggregates are formulated. The gravitational force is given by:

$$\mathbf{F}_{gi} = \mathbf{W}_i + \mathbf{F}_{bi} = \frac{4}{3}\pi a_i^3(\rho_i - \rho_b)\mathbf{g} \tag{23}$$

where ρ_i, ρ_b are the density of the particle i and of the blood respectively.

E. Van der Waals forces

Van der Waals forces act among the particles when they are not in contact. The van der Waals potential between spheres of equal radius a is given by:

$$V_{ji} = -\frac{A}{6}\left(\frac{2a^2}{\left|\mathbf{r}_{ji}\right|^2 - 4a^2} + \frac{2a^2}{\left|\mathbf{r}_{ji}\right|^2} + \ln\left(\frac{\left|\mathbf{r}_{ji}\right|^2 - 4a^2}{\left|\mathbf{r}_{ji}\right|^2}\right)\right) \tag{24}$$

where A is the Hamaker constant and $|\mathbf{r}_{ji}| \geq 2a + \delta$. The minimum distance δ to which the two surfaces can approach is assumed to be $4\,\mathring{A}$. The force is given by:

$$\mathbf{F}_{vdwij} = -\nabla V_{ji} \tag{25}$$

V. Simulation

A. Software design

A 2-D simulation platform has been developed in MATLAB. It is based on the models described in the previous section. The current status of the program allows simulation, visualization and post-processing analysis of system response. This computational tool provides the means to: (i) verify analytical results and examine parameter sensitivity, (ii) demonstrate the self-assembly properties of the system of nanoparticles and examine the drivability of the aggregations and (iii) assess the efficacy of navigation controllers.

B. Simulation examples

1) 3 particles scenario

The first simulation example aims to demonstrate: (i) that the force models produce meaningful results, (ii) how superparamagnetic nanoparticles interact in the presence of a uniform magnetic field (no external magnetic gradients exist) and (iii) to provide quantitative information on the forces developed during particle interaction. The scenario involves three particles, of radius 100 nm, initially placed at the vertices of an equilateral triangle. Fig. 7 and Fig. 8 demonstrate the history of the magnetic, and contact forces exerted on the three spheres during simulation. The left column corresponds to particle 1, the right column to particle 2 and the middle column to particle 3. It is evident that after the instant of impact the particles reach a state of equilibrium. Drag and van der Waals forces exhibit similar behavior and have been omitted.

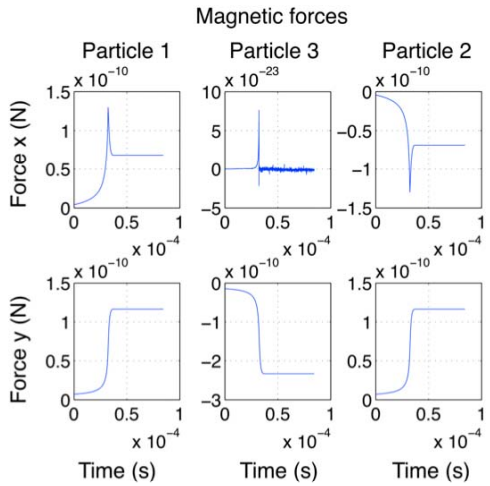

Fig. 7. History of magnetic forces.

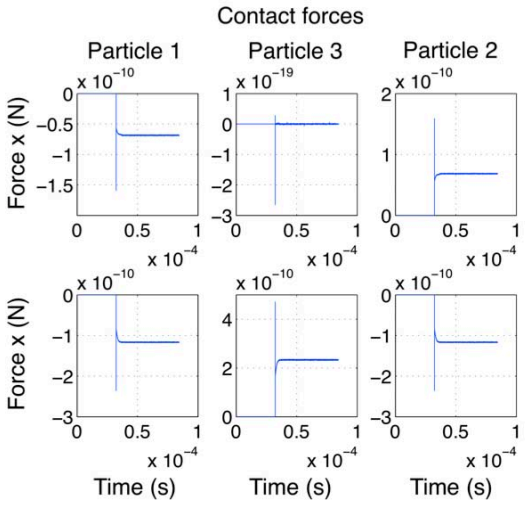

Fig. 8. History of contact forces.

2) Multi-particle scenario - no external driving forces

This scenario simulates 80 superparamagnetic particles of radius 200 nm within a blood vessel. Blood flow speed is 0.05 m/s. The external uniform static field is 3T (clinical MRI specifications) and is directed along the longitudinal axis of the vessel (positive x-direction in 11). There are no external magnetic gradients. The initial particle configuration is shown in Fig. 9. Fig. 10, Fig. 11 and Fig. 12 depict snapshots of the particles paths. Interestingly, it is observed that due to: (i) the aligning effect of the field, (ii) the competition between magnetic dipole-dipole interactions and (iii) the fluid drag effects, the nanoparticles tend to self-assemble into chains, with the magnetic dipoles aligned in a head to tail fashion and parallel to the magnetic field. In Fig. 14 the chains have acquired a bow configuration due to the laminar flow of the blood. These preliminary simulation results are in accordance with the results that have been produced in several experimental works [16, 17].

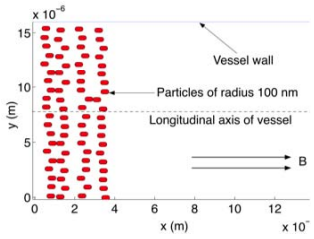

Fig. 9. Initial configuration.

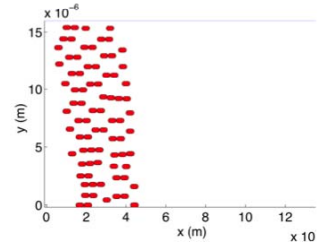

Fig. 10, configuration after 10 μs.

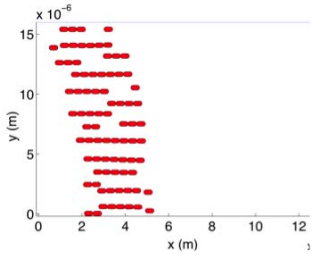

Fig. 11. Chains formulation.

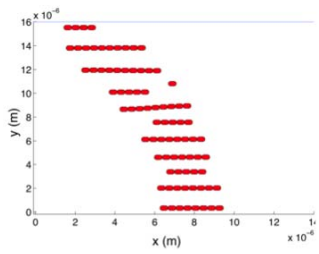

Fig. 12. Chain formulation.

VI. Conclusions & Future Work

The maximum magnetic gradient specifications of existing clinical or enhanced clinical MRI systems do not provide sufficient actuation forces to navigate magnetic nanocapsules through the arterial blood distribution system. This paper proposed a way to overcome this critical drawback through the controlled formation of micron size agglomerations, where the size can be regulated according to external stimuli (magnetic fields, temperature variation, etc.). Systematic investigation is performed through detailed modeling of the underlying physics of the inflow self-assembly process of magnetized nanoparticles. A computational tool has been developed that exploits the constructed model and performs simulation, visualization and post-processing analysis of the nanoparticle behavior within the vessel. Preliminary results have been presented demonstrating the self-assembly properties of the nanoparticles. This is a promising result that encourages further investigation on the controlled formation of magnetized nanoparticles for navigation purposes.

Future work includes further systematic study on: (i) the response of the aggregated formation as well as on the break up process, (ii) sensitivity analysis of agglomeration size, (iii) the combination of aggregation strategies and polymer encapsulation methods [12], since controlled aggregate formation will allow for substantial reduction of polymer microsphere size, (iv) the feedback control architecture for the navigation of the agglomerated nanoparticles. The simulation program will be developed further aiming at a MATLAB toolbox package that simulates feedback-controlled response of the nanoparticles. Finally, a short-term goal is to validate the results through a number of experiments that involve the inflow navigation of superparamagnetic nanoparticles using a phantom device.

References

[1] Gupta, R.B. and U.B. Kompella, 2006. "Nanoparticle Technology for Drug Delivery," Taylor & Francis, New York.

[2] Bawa, R., 2008. "Nanoparticle-based Therapeutics in Humans: A Survey, " *Nanotechnology Law & Business* 5:(2), 135-155.

[3] Arruebo, M., R. Fernandez-Pacheco, M.R. Ibarra, and J. Santamaria, 2007. "Review: Magnetic nanoparticles for drug delivery," *NanoToday* 2:(3), 22-32.

[4] Alexiou, C., R. Jurgons, C. Seliger et al., 2007. "Delivery of Superparamagnetic Nanoparticles for Local Chemotherapy after Intraarterial Infusion and Magnetic Drug Targeting," *Anticancer Research* 27, 2019-2022.

[5] Mathieu, J.-B. and S. Martel, 2007. "Magnetic microparticle steering within the constraints of an MRI system: proof of concept of a novel targeting approach", *Biomedical Microdevices* 9, 801-808.

[6] Martel, S. , J.-B. Mathieu, O. Felfoul et al., 2008. "A computer-assisted protocol for endovascular target interventions using a clinical MRI system for controlling untethered microdevices and future nanorobots," *Computed Aided Surgery* 13:(6), 340-352.

[7] Behkam, B. and M. Sitti, 2007. "Bacterial flagella-based propulsion and on/off motion control of microscale objects," *Applied Physics Letters* 90 (2), 1-3.

[8] Yesin, K.B., K. Vollmers, and B.J. Nelson, 2006. "Modeling and control of untethered biomicrorobots in a fluidic environment using electromagnetic fields," *Int J Robot Res* 25, 527-536.

[9] Walter F. Boron and Emile, L. Boulpaep, 2008. "Medical Physiology", 2nd Edition, Elsevier Health Sciences.

[10] Laurent Arcese, Matthieu Fruchard and Antoine Ferreira, "Nonlinear modeling and robust controller-observer for magnetic microrobot in a fluidic environment using MRI gradients," *Proceedings IEEE International Conference on Intelligent Robotics and Systems,* St. Louis, USA, 2009.

[11] Ralf Kehlenbeck and Renzo Di Felice, 1999, "Empirical relationship for the terminal settling velocity of spheres in cylindrical columns," *Chem. Eng. Technol*., vol. 21 (4), pp. 303-308.

[12] Pierre Pouponneau, Jean-Christophe Leroux, Sylvain Martel, "Magnetic nanoparticles encapsulated into biodegradable microparticules steered with an upgraded magnetic resonance imaging system for tumor chemo-embolization", Biomaterial 30 (2009), pp. 6327-6332.

[13] J. D. Jackson, "Classical Electrodynamics", 3rd ed., John Wiley & Sons, Inc, 1999, pp. 184-190.

[14] E. Tijskens, H. Ramon, J. De Baerdemaeker, 2003, "Discrete element for process simulation in agriculture," *Jounal of Sound and Vibration*, vol. 266, pp. 493-514.

[15] A. R. Pries, T.W. Secomb, P. Gaehtgens, 1996, "Biophysical aspects of blood flow in the microvasculature," *Cardiovascular Research*, vol. 32, pp. 654-667.

[16] M. Mastrangeli, S. Abbasi, C. Varel, C. Van Hoof, J-P Celis and K. F. Bohringer, 2009, "Self-assembly from mili- to nanoscales: methods and applications," *Journal of Micromech. Microeng*., vol. 19 (8), p. 083001.

[17] Tenase M. Silevitch D M, 2002, Hultgren A, Bauer L A, Searson P C, Meyer G J and Reich D H, "Magnetic trapping and self-assembly of multicomponent nanowires," *J. Appl. Phys.,* vol. 91, pp 8549-51.